Inkjet-printed dual-mode electrochromic and electroluminescent displays incorporating ecofriendly materials

Manuel Pietsch[a,b], *Nerea Casado*[d], *David Mecerreyes,*[d,e], *Gerardo Hernandez-Sosa*[a,b,c,]*

a. Light Technology Institute, Karlsruhe Institute of Technology, Engesserstr. 13, 76131 Karlsruhe, Germany

b. InnovationLab, Speyererstr. 4, 69115 Heidelberg, Germany

c. Institute of Microstructure Technology, Hermann-von-Helmholtz-Platz 1, 76344 Eggenstein-Leopoldshafen, Germany

d. POLYMAT University of the Basque Country UPV/EHU, Avenida de Tolosa 72, Donostia-San Sebastian 2008, Spain

e. Ikerbasque, Basque Foundation for Science, E-48011 Bilbao, Spain

KEYWORDS

dual-mode device, electrochromic devices, electrochemiluminescent devices, ecofriendly materials, inkjet-printing

ABSTRACT

Displays and indicators are an integral component of everyday electronics. However, the short-lifecycle of most applications is currently contributing to the unsustainable growth of electronic waste. In this work, we utilize ecofriendly materials in combination with sustainable processing techniques to fabricate inkjet-printed, ecofriendly dual-mode displays (DMD). These displays can be used in a reflective mode or in an emissive mode by changing between DC and AC operation due to the combination of an electrochromic (EC) and electrochemiluminescent (ECL) layer in a single device. The EC polymer PEDOT:PSS serves as the reflective layer, while a ECL gel made of dimethylsulfoxide (DMSO), poly(lactic-co-glycolic acid) (PLGA), 1-butyl-3-methylimidazoliumbis(oxalato)borate (BMIMBOB) and tris(bipyridine)ruthenium(II) chloride ($Ru^{2+}(bpy)_3Cl_2$) enables the emissive mode. The final dual-mode devices exhibit their maximum optical power output of 52mcd·m^{-2} at 4V and 40Hz, and achieved an EC contrast of 45% and a coloration efficiency of 244cm^2·C^{-1} at a wavelength of 690nm. The fabricated devices showed clear readability in dark and light conditions when operated in reflective or emissive modes. This work demonstrates the applicability of ecofriendly and potentially biodegradable materials to reduce the amount of hazardous components in versatile display technologies.

1. Introduction

An increase in the daily use of electronic devices together with missing recycling strategies is currently aggravating the impact of environmentally harmful components contained in electronic

waste.[1,23] Increasing the utilization of biodegradable, sustainable or ecofriendly materials[4] in the fabrication of electronic devices offers the possibility to lower the number of components with energy intensive, complex or hazardous end-of-life pathways (e.g. nanoparticles[5,6] or fluorinated molecules[7]). In recent years, electronic devices incorporating ecofriendly materials such as paper, β-carotene, indigo, poly(glycerol sebacate), magnesium, the poly(lactide-co-glycolide) (PLGA) into sensors,[89] batteries,[10,11] or transistors[12] have been reported. These examples demonstrate the manifold of possibilities available to create more sustainable technology.

Nowadays most electronic devices utilize displays or optical means to convey information to the user. However, there are only few reports on the use of ecofriendly materials within optoelectronic elements such as light-emitting electrochemical cells (LEC), organic light-emitting diodes (OLED), or electrochromic (EC) devices to fabricate displays or indicators.[13–18] Commonly used display technologies typically work either in a reflective mode, or in an emissive mode. An optimal display would combine both modes in form of a dual-mode display (DMD) to ensure readability, contrast and energy-efficiency in dark, as well as in light conditions. There are few examples of DMDs in literature, such as combinations of a LEC with an EC device,[19] of the electrochromic and electrofluorochromic effects of materials,[20] of fluorescent and reflective electrophoretic particles,[21] or of a liquid crystal layer with a electrochemiluminescent (ECL) devices.[22] Another promising approach realizing DMDs is to combine an ECL for light-emission and a EC device for reflective readability in one.[23] Unfortunately, none of the examples above makes use of ecofriendly materials which would be an added-value to increase the sustainability of this promising technology. In addition, the ecological footprint of displays could further be reduced by utilizing sustainable fabrication methods such as inkjet-printing, which allow low processing temperatures, low material waste and easy customizability. Due to its industrial maturity, inkjet-printing is

becoming a significant fabrication method for the cost-efficient fabrication of electronic devices and complex integrated circuits.[24–30] Recently, we have shown inkjet-printed DMDs based on the EC and electrofluorochromic properties of polyindenofluoren-8-tryarylamine, as well as an inkjet-printed electrochromic display comprised of 33 individually addressable pixels, whose biodegradability was confirmed according to international standards.[14,20] This highlights the advantages of DMDs and the sustainable benefits of ecofriendly materials when combined with the freedom of design offered by inkjet printing.

In this work, we present a novel architecture for DMDs combining electrochromic and electrochemiluminescent layers in one device and utilizing ecofriendly electrolyte and non-fluorinated light-emitting materials. The emissive and reflective modes can be enabled by switching between AC and DC operation. Incorporated between indium-tin oxide (ITO) electrodes, the presented devices comprise of the Poly-3,4-ethylendioxythiophene:polystyrene sulfonate (PEDOT:PSS) electrochromic layer and an ECL gel incorporating the non-fluorinated emitter tris(bipyridine)ruthenium(II) chloride ($Ru^{2+}(bpy)_3Cl_2$)[31], mixed into a biodegradable electrolyte system made of a non-fluorinated ionic liquid, 1-butyl-3-methylimidazolium bis(oxalato)borate (BMIMBOB), and a biodegradable polymer PLGA. The performance of the devices utilizing ecofriendly materials was investigated in terms of EC contrast, luminance, and operating conditions and compared commonly used material systems. Finally, the applicability of ecofriendly materials and fabrication methods for displays is highlighted by an inkjet-printed DMD prototype.

2. Experimental Section

2.1 Materials: $Ru^{2+}(bpy)_3PF_6$ (97%), $Ru^{2+}(bpy)_3Cl_2$ (99.95%), BMIMTFSI (≥97%), PLGA (85:15, 50k-75k) and DMSO (≥99.9%) were purchased from Sigma Aldrich. Poly(3,4-ethylenedioxythiophene):poly(styrenesulfonate) (PEDOT:PSS, FHC Solar) was obtained from Heraeus. The materials were used as received. The ITO substrates were purchased from Kintec Inc. BMIMBOB was synthesized according to Xu et al.[32]

2.2 Fabrication of the electrolyte: The ionic liquid was stirred in DMSO until it completely dissolved. Afterwards 100µl of the solution was mixed with 100mg PLGA and left on the hotplate at 50°C over night until a polymer electrolyte gel formed.

2.3 Fabrication of the electrochromic devices: The ITO coated glass substrates were cleaned for 10 minutes in acetone and isopropanol in an ultrasonication bath for. Subsequently, the substrates were treated for 5 minutes with argon plasma in a Tetra 30, Diener electronics. The substrates were coated with PEDOT:PSS by spincoating at 1600rpm for 60s with an initial acceleration of 1000 $rpms^{-1}$ to get a layer thickness of 150nm±18nm. The electrolyte gel was applied on top of the spincoated layer, before the device was finished by a second ITO coated glass slide.

2.4 Fabrication of the electrochemiluminescent devices: The electrochemiluminescent gel is based on the electrolyte gels described above. The $Ru^{2+}(bpy)_3$ was dissolved in the DMSO solution before being added to the PLGA. The ITO coated glass electrodes were cleaned as mentioned above. The electrochemiluminescent gel was sandwiched between two ITO electrodes.

2.5 Fabrication of the dual mode devices: The dual-mode devices were fabricated similar to the electrochromic devices. It only differs in using the electrochemiluminescent gel instead of the pristine electrolyte gel. For the inkjet-printed prototype, the ITO electrodes were structured by

printing negatives of the active area with PLGA as biodegradable dielectric on a Fujifilm Dimatix 2850 printer. Therefore, a 20g/l ink in anisole was used together with a customized waveform. The PEDOT:PSS layer was inkjet-printed as reported in previous work.[20]

2.6 Characterization Methods: A PGSTAT128N (AutoLab) was used to measure the I-V characteristics of the EC devices and to perform impedance spectroscopy on the electrolytes. For the UV-vis measurements an AvaSpec-ULS3648 (Avantes) and a light source ranging from 300 nm to 1100 nm were used. The measurements of the contact angles were conducted with a Krüss DSA-100 measurement setup. Layer thicknesses were measured with a profilometer from Dektak. The luminance of the ECL devices was measured in a customized integrating sphere setup with a 818-UV/DB photodiode and a OD3 attenuator connected to a 2936-R Benchtop Optical Power Meter from Newport.

3. Results and Discussion

A schematic representation of the device architecture of the dual-mode devices is presented in **Figure 1a**. It consists of two functional layers responsible for the reflective and emissive modes of the DMD sandwiched between ITO-electrodes. The emissive layer is an ECL gel, made of $Ru^{2+}(bpy)_3Cl_2$, PLGA, and BMIMBOB dissolved in dimethylsulfoxide (DMSO). In recent years, the ECL effect has become a powerful method in biosensing assays for sensing of metal ions, biomolecules and cells.[33–35] Furthermore, it has been utilized for light-emitting devices incorporating polymers or transition metal complexes emitters and an electrolyte in a single active layer.[36–40] The electrochemical nature of the ECL single-layer device makes it ideal to complement an ECD in a DMD. Thus we chose the electrochromic polymer PEDOT:PSS for the reflective layer of our device.

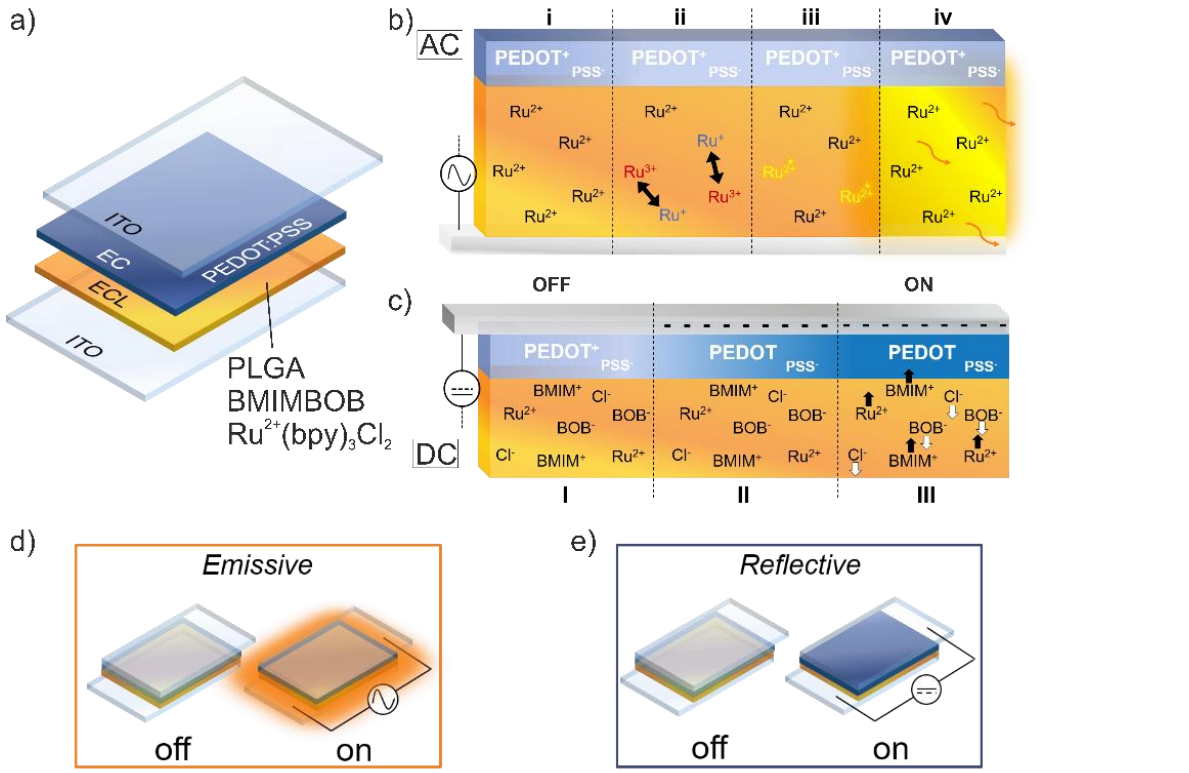

Figure 1: Schematic representation of a) the device architecture, b) the light emission process in electrochemiluminescent part of the DMD and c) the electrochromic part of the DMD. Operative modes of the DMD by switching between d) AC and e) DC.

Figure 1b shows a schematic representation of the processes inside the emissive ECL layer under operation. Herein, only one electrode of the device and the Ruthenium emitter is shown for better visualization (i). By applying an alternating voltage, some of the Ru^{2+} complexes get oxidized to Ru^{3+}, while others get reduced to Ru^{+} (ii). By chance the excess electron of the reduced species will be transferred to the oxidized species, where it can occupy an excited state (iii). This excited state will decay into the ground state while emitting the excess energy in form of light (iv). The ions of the electrolyte surrounding the emitter will maintain the electrical equilibrium during the oxidation and reduction processes. PLGA provides the mechanical properties of the gel and an increased ionic conductivity.[41,42] In a single layer device, the described processes happen at both

electrodes. In our device, the ECL gel also serves as the electrolyte for the electrochromic layer. A schematic representation of the electrochromic process is depicted in **Figure 1c**. Again, for better visualization only one electrode is depicted (I). PEDOT is in its initial oxidized state. By applying a DC potential, the polymer gets reduced and starts changing its color due to the development of new absorption bands (II). At the same time the ions inside the ECL gel, including the emitter molecules, start moving to counterbalance the space charge of the reduced PEDOT layer and the coloring gets further enhanced (III). Thus the reflective mode can be enabled by applying DC voltage which leads to a color change of the electrochromic material (**Figure 1d**). Applying an AC voltage will lead to light emission in the ECL layer to enable the emissive mode (**Figure 1e**).The two modes of the dual-mode device can be switched on by changing from an AC to a DC voltage (or vice versa). A sufficiently high frequency of the AC voltage will prevent the coloration change in the DC mode.

The most crucial part of the active layer of our dual-mode device is the electrolyte system. In literature, it is common to utilize non-degradable, fluorinated polymers and/or ionic liquids, which show good performance, but some pose a potential hazard to the environment.[43–45] In this work, we opted to fabricate the electrolyte gel based on PLGA dissolved in dimethylsulfoxide (DMSO), both of which are biodegradable, non-hazardous and used in medical applications.[46–51] As ionic species we investigated the performance of the ecofriendly salt BMIMBOB as a substitution for conventional fluorinated ionic liquids. **Figure 2a** presents the ionic conductivity of the electrolyte gel as a function of BMIMBOB concentration and its comparison to the widely used fluorinated compound 1-butyl-3-methylimidazolium bis(trifluoromethylsulfonyl)imide (BMIMTFSI) as a

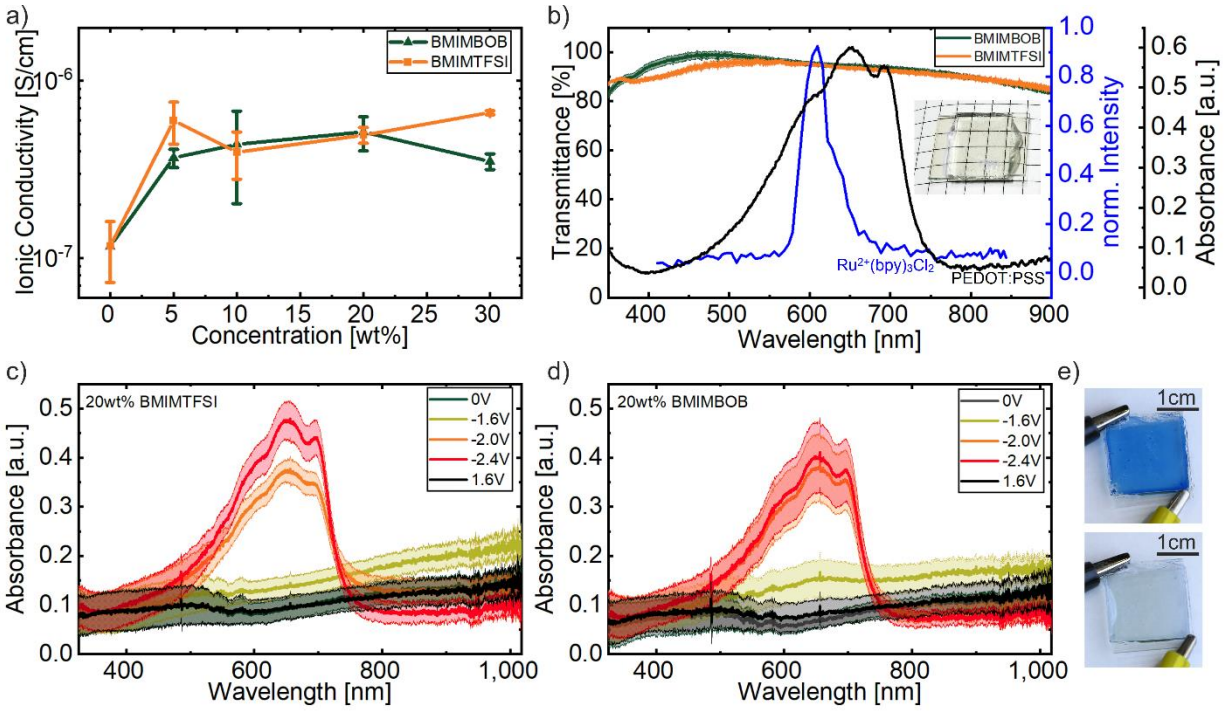

Figure 2: a) Ionic conductivity of PLGA:BMIMBOB and PLGA:BMIMTFSI electrolytes calculated from impedance measurements. b) Transmittance of PLGA:BMIMBOB and PLGA:BMIMTFSI films measured by UV-vis spectroscopy, absorbance spectrum of PEDOT:PSS and emission spectrum of $Ru^{2+}(bpy)_3$. The inset shows a photograph of the PLGA:BMIMBOB gel sandwiched between ITO coated glass slides. c) Change in absorbance of PEDOT:PSS based ECDs utilizing a PLGA:BMIMTFSI and d) a PLGA:BMIMBOB electrolyte under operation. e) Photograph of an ECD under operation utilizing the PLGA:BMIMBOB electrolyte.

reference. The PLGA-gel without any ionic liquid serves as reference. Its ionic conductivity might originate from ionic impurities. By adding 5wt% BMIMBOB the ionic conductivity of the electrolyte gel increases by more than three times compared to the PLGA-gel without the ionic liquid until reaching a maximum of $5.1\pm1.1\cdot10^{-7}$ S/cm at 20wt%. PLGA:BMIMTFSI shows a similar increase in ionic conductivity and a similar order of magnitude for the investigated range of concentrations. The reported ionic conductivity values are in line with literature reports of

PLGA based systems[41] but are of moderate magnitude compared to state-of-the-art biodegradable electrolytes.[52] In the following experiments we used the electrolyte gel with 20wt% of salt for both systems unless otherwise noted.

Another crucial characteristic of electrolyte systems used for optoelectronic devices is its optical transparency. In particular, this should match the optical properties of the materials used in the devices. **Figure 2b** shows that both PLGA:BMIMBOB and the gel utilizing the reference fluorinated compound exhibit a transmittance >83% over the whole visible spectrum extending over the absorbance of PEDOT:PSS in its colorized state and the emission spectra of $Ru^{2+}(bpy)_3Cl_2$. The inset shows a photograph of the PLGA:BMIMBOB electrolyte gel between ITO coated glass slides to highlight its transparency. This gel exhibits a transmittance of 95%±1% at the emission peak (618nm) of $Ru^{2+}(bpy)_3Cl_2$ and a transmittance of 94%±1% at the maximum absorbance of PEDOT:PSS (653nm). The exhibited ionic conductivity together with the outstanding transparency make the ecofriendly PLGA:BMIMBOB electrolyte ideal for optoelectronic devices.

To characterize the performance of the PLGA:BMIMBOB gel in an electrochromic device, we fabricated bi-layer devices sandwiched between ITO-electrodes with PEDOT:PSS as the electrochromic layer. Devices utilizing PLGA:BMIMTFSI as electrolyte served as reference samples. The change in absorbance while applying a direct voltage of up to -2.4V for EC devices containing the PLGA: BMIMTFSI and the PLGA:BMIMBOB electrolytes are depicted in **Figure 2c** and **Figure 2d**, respectively. For both electrolytes the electrochromic devices show the main change in absorbance after exceeding 1.6 V and a reversible color switch by inverting the polarization of the direct voltage. Photographs of an electrochromic device under operation containing the ecofriendly PLGA:BMIMBOB electrolyte are presented in Figure 2e. The figures

of merit averaged over 3 ECDs for both electrolytes are listed in Table 1. The devices with the PLGA:BMIMBOB electrolyte show an electrochromic contrast of 45%±6% and a coloration efficiency of 237±89 cm²/C while the reference with BMIMTFSI exhibits an electrochromic contrast of 47%±2% and a coloration efficiency of 217±81 cm²/C at a wavelength of 690nm. The coloring switching times of both device types are below 1s. Thus we observed no drawbacks in the performance of the ECD when using the ecofriendly electrolyte compared to the fluorinated reference. More advanced EC device architectures include ion storage layers or optimized electrodes.[53] However we opted for a simplified architecture for the DMDs as the ECL devices are based on ITO electrodes

Table 1: Figures of merit of an ECD with an electrolyte gel containing BMIMTFSI versus BMIMBOB in a sandwich-type device architecture with ITO electrodes and the electrochromic part of the dual mode devices.

	Electrochromic Contrast in [%]	**Col. Efficiency in [cm²/C]**	**Switch. time$_{col}$ in [s]**	**Switch. time$_{bleach}$ in [s]**
PLGA:BMIMTFSI	47 ±2	217±81	0.92±0.05	3.78±1.79
PLGA:BMIMBOB	45±6	237±89	0.98±0.03	2.31±0.09
DMD, EC mode	45±8	244±29	0.74±0.05	2.0±0.2

We furthermore investigated the performance of the ecofriendly PLGA:BMIMBOB electrolyte gel in single layer ECL devices. For this, we blended the non-fluorinated Ruthenium-based emitter, $Ru^{2+}(bpy)_3Cl_2$ at ratios between 1wt% - 50wt% to form an ECL gel. As a reference we fabricated and characterized ECL devices utilizing PLGA:BMIMTFSI and the commonly used fluorinated

emitter tris(bipyridine)ruthenium(II) hexafluorophosphate ($Ru^{2+}(bpy)_3PF_6$).[54] The electrochemically driven light emission was characterized in a customized integrating sphere setup with a connected power meter to measure the overall emission output. **Figure 3** presents the characterization of the ECL emission at different salt:emitter weight ratios between 1wt% and 50wt%. The devices were characterized in terms of luminance as a function of applied alternating voltage at a constant frequency (40 Hz) and emitted optical power normalized over all emitter ratios as a function of frequency at an alternating voltage of 4V.

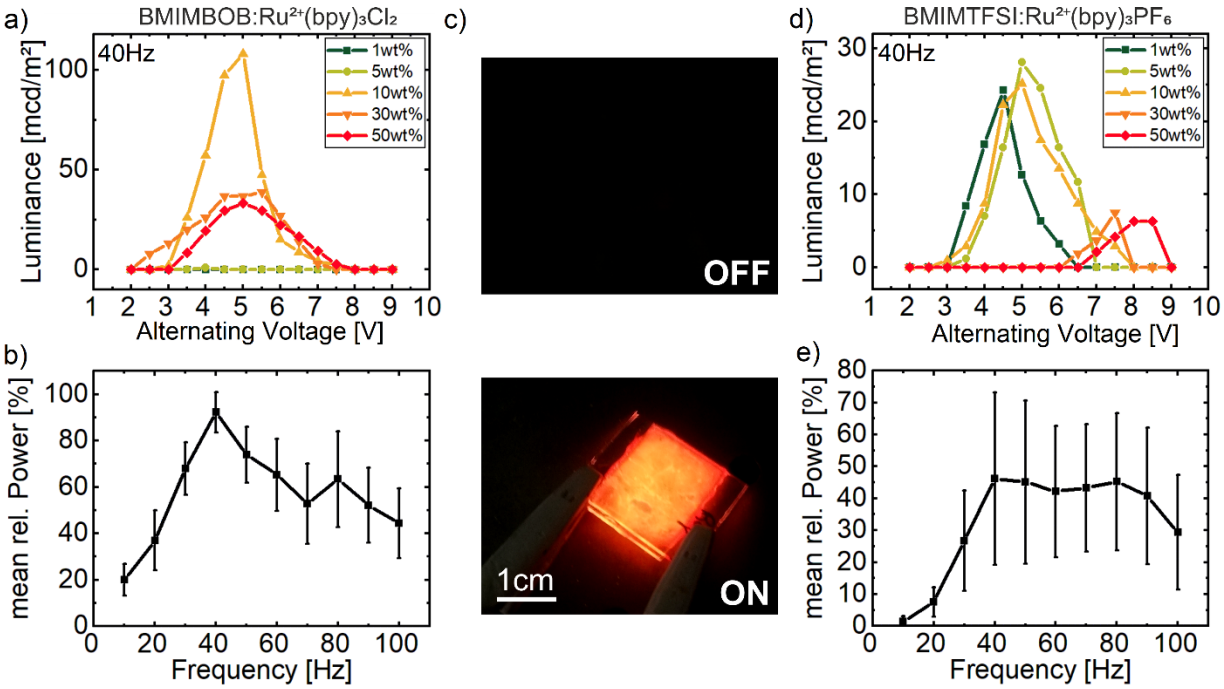

Figure 3: ECL device performance under operation by varying voltage and frequency. a) Luminance and b) mean normalized optical power of $Ru^{2+}(bpy)_3Cl_2$/PLGA/BMIMBOB in dependence of the applied alternating voltage and frequency respectively. c) Picture of the ECL device with $Ru^{2+}(bpy)_3Cl_2$/BMIMBOB under operation at 4V and 40Hz. d) Luminance and e) mean normalized optical power $Ru^{2+}(bpy)_3PF_6$/PLGA/BMIMTFSI in dependence of the applied alternating voltage and frequency respectively.

The emission properties of ECL devices with PLGA:BMIMBOB:$Ru^{2+}(bpy)_3Cl_2$ are presented in **Figure 3a**. The devices show light emission at emitter concentrations of 10wt% and beyond. The peak luminance of 108 mcd/m² was measured at an alternating voltage of 5V (40Hz) with a concentration of 10wt%. The 10wt% concentration was therefore used in the dual-mode devices. The frequency dependence of the normalized optical power averaged over all five ECL devices with BMIMBOB:$Ru^{2+}(bpy)_3Cl_2$ is depicted in **Figure 3b**. Some of them showed a rapid decrease in performance when increasing frequency above 50Hz, which caused a large spread in standard deviation. The peak optical power output is increasing alongside with the frequency up to a

maximum at 40Hz. At higher frequencies the optical power output is decreasing, therefore, we did not considered necessary to go beyond 100 Hz neither for this sample nor for the fluorinated reference compound. A picture of the PLGA:BMIMBOB:$Ru^{2+}(bpy)_3Cl_2$ device under operation at 4V and 40Hz is depicted in **Figure 3c**. The pictures show the on and off state of the device. Despite the low luminance values, the contrast between the on and the off state is clearly visible.

To further evaluate the optical performance of the PLGA:BMIMBOB:$Ru^{2+}(bpy)_3Cl_2$ devices we used a material system with the well-known emitter $Ru^{2+}(bpy)_3PF_6$ and BMIMTFSI inside the PLGA-gel as reference. The luminance in dependence of the applied alternating voltage of the reference device is depicted in **Figure 3d**. In contrast to the devices with PLGA:BMIMBOB:$Ru^{2+}(bpy)_3Cl_2$, we observed that emitter concentrations up to 10wt% work best. A maximum luminance of 28.1 mcd/m² was measured for the concentration of 5wt% at an alternating voltage of 5V. Its maximum luminance is more than three times lower than for the ecofriendly PLGA:BMIMBOB:$Ru^{2+}(bpy)_3Cl_2$. As shown in **Figure 3e**, the maximum optical power output in dependence of the frequency is located between 40Hz and 80Hz. In summary, we were able to successfully substitute all components of an ECL device with non-fluorinated, ecofriendly and biodegradable materials, while additionally enhancing its optical performance in comparison to well-known material systems. For completeness, a device with the combination of the ecofriendly ionic liquid BMIMBOB and the well-known emitter $Ru^{2+}(bpy)_3PF_6$, was also characterized in terms of luminance and frequency dependence. The results are presented in Figure S1 in the SI. This combination of materials exhibits the highest luminance of 49 mcd/m² at an

alternating voltage of 4.5V at a concentration of 5wt% and a similar frequency dependence as the other devices.

In the next successive step, we demonstrate the combination of the EC and the ECL layer in one single dual-mode device which operational modes can be changed by switching between alternating and direct voltage. **Figure 4a** presents the luminance of the dual-mode device averaged over three samples as a function of AC voltage operated at 40Hz. The maximum luminance of 52±19mcd/m² was measured at 4V, while the overall luminance follows the same trend as in the single device. Also the frequency response shown in **Figure 4b** follows the same trend as in the

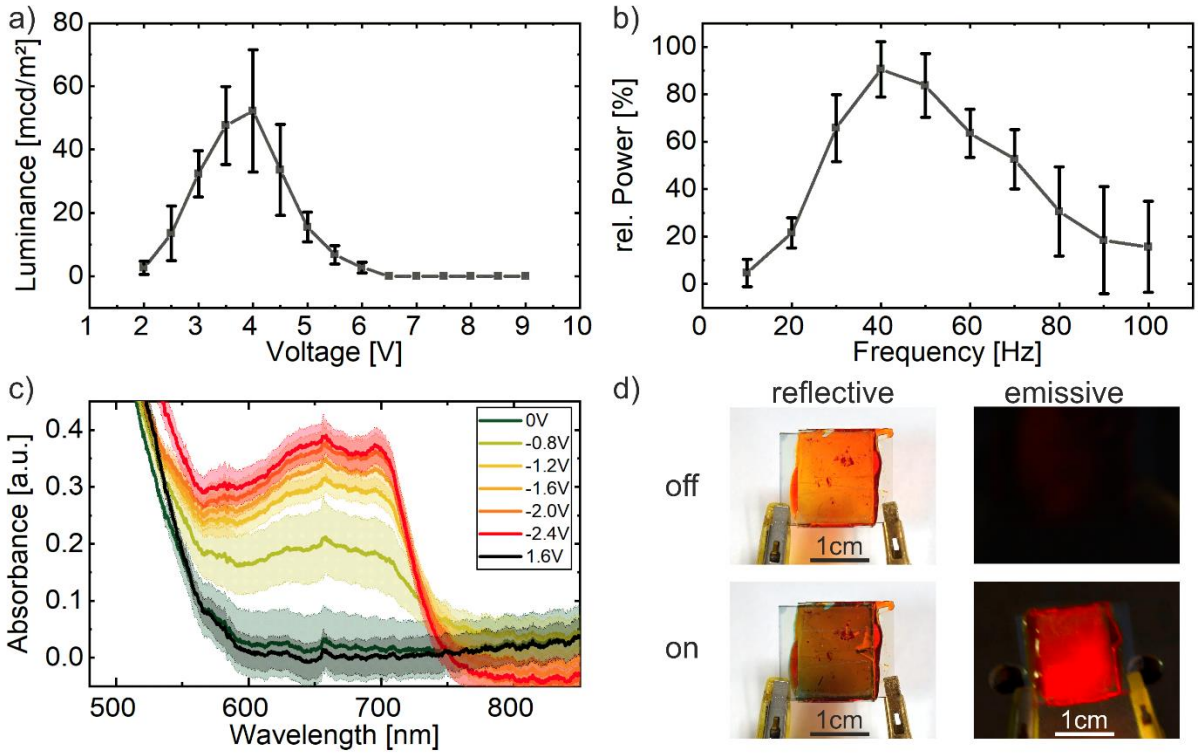

Figure 4: a) Luminance of the DMD device at varying voltage in the emissive mode. b) Relative change in emission of the DMD by varying the frequency in the emissive mode. c) Change in absorbance under operation in the reflective mode. d) Photographs of the DMD under operation in its emissive and reflective mode.

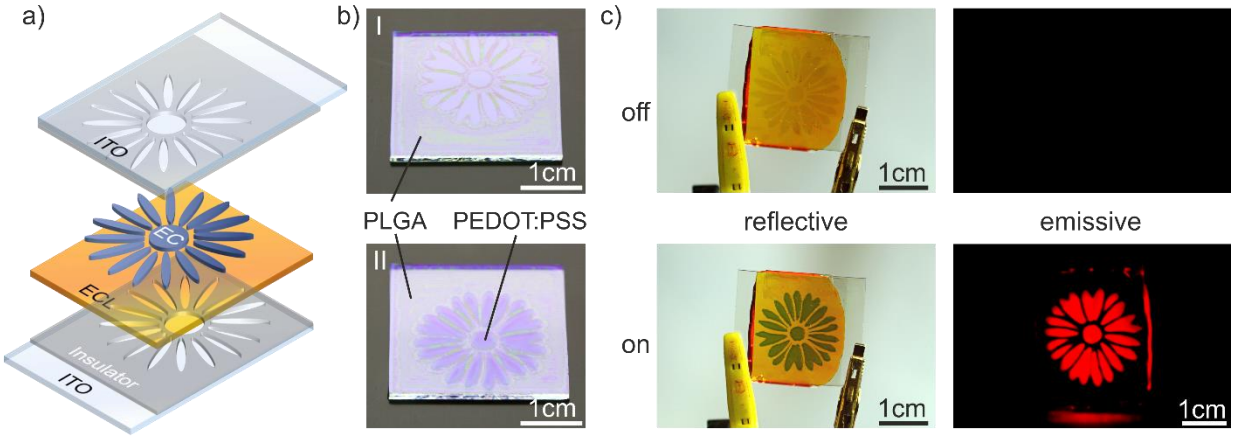

Figure 5: a) Schematic representation of the device architecture of the inkjet-printed DMD. b) Photographs of the inkjet-printing steps to structure the ITO-electrodes and the electrochromic PEDOT:PSS layer. c) Photographs of the DMD in its different operative modes.

single device (Figure 3e) with a maximum optical power output at 40Hz. Even though the luminance is not comparable to optimized displays, it is clearly visible. Future investigation of biodegradable material systems with better ionic mobility, the morphological optimization of the material blends to avoid luminescence quenching as well as the implementation of advanced device architectures could help enhancing the overall emission output of the DMD.[41,55,56] The change in absorbance of the EC layer in the dual-mode device is depicted in **Figure 4c**. In comparison to the single device (Figure 2d) there is a broader absorption in the colorized state and less distinguishable single peaks at -2.4V. The increase in absorbance below 500nm originates from the contribution of $Ru^{2+}(bpy)_3Cl_2$. The EC mode of the device shows a contrast of 45±8% and a coloration efficiency of 244±29cm²/C which are similar to the single layer device (Table 1). The dual mode device exhibited improved switching times for coloring (0.74±0.05s) and bleaching (2.0±0.2s). This improvement in operational speed might originate from the ionic nature of the emitter in the electrolyte, since it acts as additional ions.

Finally, we fabricated structured DMDs by inkjet-printing PEDOT:PSS and pre-structuring both ITO substrates before the deposition of the EC and ECL materials with an insulating PLGA layer. **Figure 5a** shows a schematic representation of the device architecture of the inkjet-printed DMD. The ITO electrodes were covered with an insulating layer of biodegradable PLGA to prevent the contact between these ITO areas to the ECL layer. Therefore, these areas will not emit light when an alternating voltage is applied and a structured light-emission can be achieved. The inkjet-printing steps are shown in **Figure 5b**. In a first step the insulating PLGA layer was printed on top of the ITO electrodes, which exhibits a layer thickness of 120±20nm (I). Thereafter, the electrochromic PEDOT:PSS layer was printed on the uncovered areas of one of the ITO electrodes (II). The utilized digital printing layouts and the contact angles of the inks are depicted in Figure S2 in the SI. The measured contact angles indicate a beneficial wetting behavior of the inks. The DMD was completed by sandwiching the ecofriendly ECL gel between the structured ITO-electrodes. **Figure 5c** shows the final inkjet-printed DMD under operation in its emissive (4V, 40 Hz) and reflective mode (-2.4V). In reflective mode the printed pattern in from of a flower is easily distinguishable under direct light due to the high contrast between the blue hue of PEDOT:PSS on the orange background of the emissive layer. In the off-state the printed structure is barely visible. In the on-state of the emissive mode the flower pattern is clearly visible in dark conditions and exhibits the characteristic red emission of $Ru^{2+}(bpy)_3Cl_2$. The operational DMD are a proof-of-concept for the proposed device architecture and the incorporation of biodegradable and ecofriendly materials. Nevertheless, the investigation of the lifetime of the devices, as well as the optimization of the utilized materials and layers to improve the device performance is part of future research. Additionally, ruthenium is a scarce metal and some of its complexes are toxic.[57] Even if

it only accounts for 2 % of the mass of the active layer, the investigation of biofriendly emitters or Cu-based complexes in future work would benefit the overall sustainability of the DMDs.[58,59]

4. Conclusion

In summary, we presented a novel device architecture for fabricating ecofriendly dual mode devices combining EC and ECL layers. The emissive and reflective mode can be switched by changing between direct and alternate voltage operation. Furthermore, we demonstrated and inkjet-printed DMD capable of displaying static images. The device was comprised an electrolyte was based on the ecofriendly materials PLGA:BMIMBOB, the electrochromic biocompatible material PEDOT:PSS and the non-fluorinated light-emitting compound $Ru^{2+}(bpy)_3Cl_2$. The devices exhibited a luminance of 52±19mcd/m² at 4V and 40Hz, a contrast of 45±8% and a coloration efficiency of 244±29cm²/C, which did not represent any loss of performance compared to the single EC or ECL reference devices. Furthermore, the switching times for coloring and bleaching of the electrochromic mode were improved down to 2.0±0.2s and 0.74±0.05s, respectively. These results highlight the utilization of biodegradable and ecofriendly materials for the fabrication of cost-efficient displays suitable for high-throughput production and a large variety of short-lifecycle applications. Further work should focus on the investigation of high-performance material systems that enable fully biodegradable DMDs contributing to the reduction of electronic waste.

ASSOCIATED CONTENT

Supporting Information is available online or from the author.

- Formulas for calculating the luminance of the devices in the integrating sphere setup

- Luminance vs. voltage and optical power vs. frequency of an additional ECL device reference with $Ru^{2+}(bpy)_3PF_6$/PLGA/BMIMBOB
- Printing images for the dual-mode displays and contact angle measurements of the used inks.
- Current of the electrochromic layers when switching back and forth

AUTHOR INFORMATION

Corresponding Author

Gerardo Hernandez-Sosa

gerardo.sosa@kit.edu

Notes

The authors declare no competing financial interest.

ACKNOWLEDGMENT

This project was partially supported by the German Federal Ministry of Education and Research (BMBF) through Grant FKZ: 03X5526. N.C. and D.M. would like to thank AEI-MINECO for financial support through project PID2020-119026GB-I00.

ABBREVIATIONS

BMIMBOB, 1-butyl-3-methylimidazolium bis(oxalato)borate; BMIMTFSI, 1-butyl-3-methylimidazolium bis(trifluoromethylsulfonyl)imide; DMD, dual-mode display; EC, electrochromic; ITO, indium-tin oxide; LEC, light-emitting electrochemical cell; OLED, organic light-emitting diode; PEDOT:PSS, poly-3,4-ethylendioxythiophene:polystyrene sulfonate; PLGA,

poly(lactide-co-glycolide); $Ru^{2+}(bpy)_3Cl_2$, tris(bipyridine)ruthenium(II) chloride ; $Ru^{2+}(bpy)_3PF_6$, tris(bipyridine)ruthenium(II) hexafluorophosphate;

REFERENCES

(1) Balde, C. P.; Forti, V.; Gray, V.; Kuehr, R.; Stegmann, P. *The Global E-Waste Monitor 2017*; 2017. https://doi.org/10.1016/j.proci.2014.05.148.

(2) Wang, Z.; Zhang, B.; Guan, D. Take Responsibility for Electronic-Waste Disposal. *Nature* **2016**, *536* (7614), 23–25. https://doi.org/10.1038/536023a.

(3) Tansel, B. From Electronic Consumer Products to E-Wastes: Global Outlook, Waste Quantities, Recycling Challenges. *Environ. Int.* **2017**, *98*, 35–45. https://doi.org/10.1016/j.envint.2016.10.002.

(4) Irimia-Vladu, M.; Głowacki, E. D.; Voss, G.; Bauer, S.; Sariciftci, N. S. Green and Biodegradable Electronics. *Mater. Today* **2012**, *15* (7–8), 340–346. https://doi.org/10.1016/S1369-7021(12)70139-6.

(5) Tortella, G. R.; Rubilar, O.; Durán, N.; Diez, M. C.; Martínez, M.; Parada, J.; Seabra, A. B. Silver Nanoparticles: Toxicity in Model Organisms as an Overview of Its Hazard for Human Health and the Environment. *J. Hazard. Mater.* **2020**, *390* (November 2019), 121974. https://doi.org/10.1016/j.jhazmat.2019.121974.

(6) Turan, N. B.; Erkan, H. S.; Engin, G. O.; Bilgili, M. S. Nanoparticles in the Aquatic Environment: Usage, Properties, Transformation and Toxicity—A Review. *Process Saf. Environ. Prot.* **2019**, *130*, 238–249. https://doi.org/10.1016/j.psep.2019.08.014.

(7) Zhang, C.; Yan, K.; Fu, C.; Peng, H.; Hawker, C. J.; Whittaker, A. K. Biological Utility of Fluorinated Compounds: From Materials Design to Molecular Imaging, Therapeutics and Environmental Remediation. *Chem. Rev.* **2022**, *122* (1), 167–208. https://doi.org/10.1021/acs.chemrev.1c00632.

(8) Boutry, C. M.; Nguyen, A.; Lawal, Q. O.; Chortos, A.; Rondeau-Gagné, S.; Bao, Z. A Sensitive and Biodegradable Pressure Sensor Array for Cardiovascular Monitoring. *Adv. Mater.* **2015**, *27* (43), 6954–6961. https://doi.org/10.1002/adma.201502535.

(9) Salvatore, G. A.; Sülzle, J.; Dalla Valle, F.; Cantarella, G.; Robotti, F.; Jokic, P.; Knobelspies, S.; Daus, A.; Büthe, L.; Petti, L.; Kirchgessner, N.; Hopf, R.; Magno, M.; Tröster, G. Biodegradable and Highly Deformable Temperature Sensors for the Internet of Things. *Adv. Funct. Mater.* **2017**, *27* (35), 1702390. https://doi.org/10.1002/adfm.201702390.

(10) Huang, X.; Wang, D.; Yuan, Z.; Xie, W.; Wu, Y.; Li, R.; Zhao, Y.; Luo, D.; Cen, L.; Chen, B.; Wu, H.; Xu, H.; Sheng, X.; Zhang, M.; Zhao, L.; Yin, L. A Fully Biodegradable Battery for Self-Powered Transient Implants. *Small* **2018**, *14* (28), 1800994. https://doi.org/10.1002/smll.201800994.

(11) Jia, X.; Wang, C.; Ranganathan, V.; Napier, B.; Yu, C.; Chao, Y.; Forsyth, M.; Omenetto, F. G.; Macfarlane, D. R.; Wallace, G. G. A Biodegradable Thin-Film Magnesium Primary Battery Using Silk Fibroin-Ionic Liquid Polymer Electrolyte. *ACS Energy Lett.* **2017**, *2* (4), 831–836. https://doi.org/10.1021/acsenergylett.7b00012.

(12) Irimia-Vladu, M.; Troshin, P. A.; Reisinger, M.; Shmygleva, L.; Kanbur, Y.; Schwabegger,

G.; Bodea, M.; Schwödiauer, R.; Mumyatov, A.; Fergus, J. W.; Razumov, V. F.; Sitter, H.; Sariciftci, N. S.; Bauer, S. Biocompatible and Biodegradable Materials for Organic Field-Effect Transistors. *Adv. Funct. Mater.* **2010**, *20* (23), 4069–4076. https://doi.org/10.1002/adfm.201001031.

(13) Jürgensen, N.; Zimmermann, J.; Morfa, A. J.; Hernandez-Sosa, G. Biodegradable Polycaprolactone as Ion Solvating Polymer for Solution-Processed Light-Emitting Electrochemical Cells. *Sci. Rep.* **2016**, *6* (1), 36643. https://doi.org/10.1038/srep36643.

(14) Pietsch, M.; Schlisske, S.; Held, M.; Strobel, N.; Wieczorek, A.; Hernandez-Sosa, G. Biodegradable Inkjet-Printed Electrochromic Display for Sustainable Short-Lifecycle Electronics. *J. Mater. Chem. C* **2020**, *8* (47), 16716–16724. https://doi.org/10.1039/D0TC04627B.

(15) Jürgensen, N.; Ackermann, M.; Marszalek, T.; Zimmermann, J.; Morfa, A. J.; Pisula, W.; Bunz, U. H. F.; Hinkel, F.; Hernandez-Sosa, G. Solution-Processed Bio-OLEDs with a Vitamin-Derived Riboflavin Tetrabutyrate Emission Layer. *ACS Sustain. Chem. Eng.* **2017**, *5* (6), 5368–5372. https://doi.org/10.1021/acssuschemeng.7b00675.

(16) Zimmermann, J.; Porcarelli, L.; Rödlmeier, T.; Sanchez-Sanchez, A.; Mecerreyes, D.; Hernandez-Sosa, G. Fully Printed Light-Emitting Electrochemical Cells Utilizing Biocompatible Materials. *Adv. Funct. Mater.* **2018**, *28* (24), 1705795. https://doi.org/10.1002/adfm.201705795.

(17) Cavinato, L. M.; Millán, G.; Fernández-Cestau, J.; Fresta, E.; Lalinde, E.; Berenguer, J. R.; Costa, R. D. Versatile Biogenic Electrolytes for Highly Performing and Self-stable Light-

emitting Electrochemical Cells. *Adv. Funct. Mater.* **2022**, 2201975. https://doi.org/10.1002/adfm.202201975.

(18) Chaudhary, A.; Pathak, D. K.; Kandpal, S.; Ghosh, T.; Tanwar, M.; Kumar, R. Raw Hibiscus Extract as Redox Active Biomaterial for Novel Herbal Electrochromic Device. *Sol. Energy Mater. Sol. Cells* **2020**, *215* (January), 110588. https://doi.org/10.1016/j.solmat.2020.110588.

(19) Wang, X. J.; Lau, W. M.; Wong, K. Y. Display Device with Dual Emissive and Reflective Modes. *Appl. Phys. Lett.* **2005**, *87* (11), 1–4. https://doi.org/10.1063/1.2043249.

(20) Pietsch, M.; Rödlmeier, T.; Schlisske, S.; Zimmermann, J.; Romero-Nieto, C.; Hernandez-Sosa, G. Inkjet-Printed Polymer-Based Electrochromic and Electrofluorochromic Dual-Mode Displays. *J. Mater. Chem. C* **2019**, *7* (23), 7121–7127. https://doi.org/10.1039/C9TC01344J.

(21) Hong, J.; Lai, M.; Chen, J.; Zhou, L.; Sun, T.; Ma, B.; Chen, Y.; Zeng, X.; Wu, M. Dual-Mode Chromatic Electrophoretic Display: A Prospective Technology Based on Fluorescent Electrophoretic Particles. *Chem. Eng. J.* **2022**, *439* (February), 135726. https://doi.org/10.1016/j.cej.2022.135726.

(22) Tsuneyasu, S.; Nakamura, K.; Kobayashi, N. Electroresponsive Dual Functional Display Device Enabling Both Emissive and Reflective Modes by Combining Electrochemiluminescent and Liquid Crystal Materials. *Chem. Lett.* **2016**, *45* (8), 949–951. https://doi.org/10.1246/cl.160361.

(23) Watanabe, Y.; Nakamura, K.; Kobayashi, N. Improvement in Reflective–Emissive Dual-

Mode Properties of Electrochemical Displays by Electrode Modification. *Phys. Chem. Chem. Phys.* **2011**, *13* (43), 19420. https://doi.org/10.1039/c1cp22191d.

(24) Zhan, Z.; An, J.; Wei, Y.; Tran, V. T.; Du, H. Inkjet-Printed Optoelectronics. *Nanoscale* **2017**, *9* (3), 965–993. https://doi.org/10.1039/C6NR08220C.

(25) Khan, Y.; Thielens, A.; Muin, S.; Ting, J.; Baumbauer, C.; Arias, A. C. A New Frontier of Printed Electronics: Flexible Hybrid Electronics. *Adv. Mater.* **2020**, *32* (15), 1905279. https://doi.org/10.1002/adma.201905279.

(26) Huang, Q.; Zhu, Y. Printing Conductive Nanomaterials for Flexible and Stretchable Electronics: A Review of Materials, Processes, and Applications. *Adv. Mater. Technol.* **2019**, *4* (5), 1800546. https://doi.org/10.1002/admt.201800546.

(27) Schlisske, S.; Raths, S.; Ruiz-Preciado, L. A.; Lemmer, U.; Exner, K.; Hernandez-Sosa, G. Surface Energy Patterning for Ink-Independent Process Optimization of Inkjet-Printed Electronics. *Flex. Print. Electron.* **2021**, *6* (1), 015002. https://doi.org/10.1088/2058-8585/abcc79.

(28) Merklein, L.; Daume, D.; Braig, F.; Schlisske, S.; Rödlmeier, T.; Mink, M.; Kourkoulos, D.; Ulber, B.; Di Biase, M.; Meerholz, K.; Hernandez-Sosa, G.; Lemmer, U.; Sauer, H.; Dörsam, E.; Scharfer, P.; Schabel, W. Comparative Study of Printed Multilayer OLED Fabrication through Slot Die Coating, Gravure and Inkjet Printing, and Their Combination. *Colloids and Interfaces* **2019**, *3* (1), 32. https://doi.org/10.3390/colloids3010032.

(29) Eggenhuisen, T. M.; Galagan, Y.; Biezemans, A. F. K. V.; Slaats, T. M. W. L.; Voorthuijzen, W. P.; Kommeren, S.; Shanmugam, S.; Teunissen, J. P.; Hadipour, A.;

Verhees, W. J. H.; Veenstra, S. C.; Coenen, M. J. J.; Gilot, J.; Andriessen, R.; Groen, W. A. High Efficiency, Fully Inkjet Printed Organic Solar Cells with Freedom of Design. *J. Mater. Chem. A* **2015**, *3* (14), 7255–7262. https://doi.org/10.1039/C5TA00540J.

(30) Kwon, J.; Baek, S.; Lee, Y.; Tokito, S.; Jung, S. Layout-to-Bitmap Conversion and Design Rules for Inkjet-Printed Large-Scale Integrated Circuits. *Langmuir* **2021**, *37* (36), 10692–10701. https://doi.org/10.1021/acs.langmuir.1c01296.

(31) Moon, H. C.; Lodge, T. P.; Frisbie, C. D. Solution-Processable Electrochemiluminescent Ion Gels for Flexible, Low-Voltage, Emissive Displays on Plastic. *J. Am. Chem. Soc.* **2014**, *136* (9), 3705–3712. https://doi.org/10.1021/ja5002899.

(32) Xu, W.; Wang, L.-M.; Nieman, R. A.; Angell, C. A. Ionic Liquids of Chelated Orthoborates as Model Ionic Glassformers. *J. Phys. Chem. B* **2003**, *107* (42), 11749–11756. https://doi.org/10.1021/jp034548e.

(33) Ma, C.; Cao, Y.; Gou, X.; Zhu, J.-J. Recent Progress in Electrochemiluminescence Sensing and Imaging. *Anal. Chem.* **2020**, *92* (1), 431–454. https://doi.org/10.1021/acs.analchem.9b04947.

(34) Babamiri, B.; Bahari, D.; Salimi, A. Highly Sensitive Bioaffinity Electrochemiluminescence Sensors: Recent Advances and Future Directions. *Biosens. Bioelectron.* **2019**, *142* (July), 111530. https://doi.org/10.1016/j.bios.2019.111530.

(35) Zanut, A.; Fiorani, A.; Rebeccani, S.; Kesarkar, S.; Valenti, G. Electrochemiluminescence as Emerging Microscopy Techniques. *Anal. Bioanal. Chem.* **2019**, *411* (19), 4375–4382. https://doi.org/10.1007/s00216-019-01761-x.

(36) Oh, H.; Seo, D. G.; Moon, H. C. Performance Improvement of Yellow Emitting Electrochemiluminescence Devices: Effects of Frequency Control and Coreactant Pathway. *Org. Electron.* **2019**, *65* (November 2018), 394–400. https://doi.org/10.1016/j.orgel.2018.11.043.

(37) Hwang, H.; Kim, J. K.; Moon, H. C. Improvement of Brightness, Color Purity, and Operational Stability of Electrochemiluminescence Devices with Diphenylanthracene Derivatives. *J. Mater. Chem. C* **2017**, *5* (47), 12513–12519. https://doi.org/10.1039/C7TC03389C.

(38) Soulsby, L. C.; Doeven, E. H.; Pham, T. T.; Eyckens, D. J.; Henderson, L. C.; Long, B. M.; Guijt, R. M.; Francis, P. S. Colour Tuning and Enhancement of Gel-Based Electrochemiluminescence Devices Utilising Ru(<scp>ii</Scp>) and Ir(<scp>iii</Scp>) Complexes. *Chem. Commun.* **2019**, *55* (76), 11474–11477. https://doi.org/10.1039/C9CC05031K.

(39) Daimon, T.; Nihei, E. Fabrication of Organic Electrochemiluminescence Devices with π-Conjugated Polymer Materials. *J. Mater. Chem. C* **2013**, *1* (16), 2826. https://doi.org/10.1039/c3tc30240g.

(40) Kong, S. H.; Lee, J. I.; Kim, S.; Kang, M. S. Light-Emitting Devices Based on Electrochemiluminescence: Comparison to Traditional Light-Emitting Electrochemical Cells. *ACS Photonics* **2018**, *5* (2), 267–277. https://doi.org/10.1021/acsphotonics.7b00864.

(41) Zimmermann, J.; Jürgensen, N.; Morfa, A. J.; Wang, B.; Tekoglu, S.; Hernandez-Sosa, G. Poly(Lactic- Co -Glycolic Acid) (PLGA) as Ion-Conducting Polymer for Biodegradable

Light-Emitting Electrochemical Cells. *ACS Sustain. Chem. Eng.* **2016**, *4* (12), 7050–7055. https://doi.org/10.1021/acssuschemeng.6b01953.

(42) Kwon, W.; Chang, Y.-J.; Park, Y.-C.; Jang, H. M.; Rhee, S.-W. A Light Scattering Polymer Gel Electrolyte for High Performance Dye-Sensitized Solar Cells. *J. Mater. Chem.* **2012**, *22* (13), 6027. https://doi.org/10.1039/c2jm15889b.

(43) Henry, B. J.; Carlin, J. P.; Hammerschmidt, J. A.; Buck, R. C.; Buxton, L. W.; Fiedler, H.; Seed, J.; Hernandez, O. A Critical Review of the Application of Polymer of Low Concern and Regulatory Criteria to Fluoropolymers. *Integr. Environ. Assess. Manag.* **2018**, *14* (3), 316–334. https://doi.org/10.1002/ieam.4035.

(44) Vieira, N. S. M.; Stolte, S.; Araújo, J. M. M.; Rebelo, L. P. N.; Pereiro, A. B.; Markiewicz, M. Acute Aquatic Toxicity and Biodegradability of Fluorinated Ionic Liquids. *ACS Sustain. Chem. Eng.* **2019**, *7* (4), 3733–3741. https://doi.org/10.1021/acssuschemeng.8b03653.

(45) Wang, Y.; Chang, W.; Wang, L.; Zhang, Y.; Zhang, Y.; Wang, M.; Wang, Y.; Li, P. A Review of Sources, Multimedia Distribution and Health Risks of Novel Fluorinated Alternatives. *Ecotoxicol. Environ. Saf.* **2019**, *182* (May), 109402. https://doi.org/10.1016/j.ecoenv.2019.109402.

(46) Hwang, S.-C. J.; Wu, J.-Y.; Lin, Y.-H.; Wen, I.-C.; Hou, K.-Y.; He, S.-Y. Optimal Dimethyl Sulfoxide Biodegradation Using Activated Sludge from a Chemical Plant. *Process Biochem.* **2007**, *42* (10), 1398–1405. https://doi.org/10.1016/j.procbio.2007.07.013.

(47) Matira, E. M.; Chen, T.-C.; Lu, M.-C.; Dalida, M. L. P. Degradation of Dimethyl Sulfoxide through Fluidized-Bed Fenton Process. *J. Hazard. Mater.* **2015**, *300*, 218–226.

https://doi.org/10.1016/j.jhazmat.2015.06.069.

(48) Danhier, F.; Ansorena, E.; Silva, J. M.; Coco, R.; Le Breton, A.; Préat, V. PLGA-Based Nanoparticles: An Overview of Biomedical Applications. *J. Control. Release* **2012**, *161* (2), 505–522. https://doi.org/10.1016/j.jconrel.2012.01.043.

(49) Bee, S.-L.; Hamid, Z. A. A.; Mariatti, M.; Yahaya, B. H.; Lim, K.; Bee, S.-T.; Sin, L. T. Approaches to Improve Therapeutic Efficacy of Biodegradable PLA/PLGA Microspheres: A Review. *Polym. Rev.* **2018**, *58* (3), 495–536. https://doi.org/10.1080/15583724.2018.1437547.

(50) Elmowafy, E. M.; Tiboni, M.; Soliman, M. E. Biocompatibility, Biodegradation and Biomedical Applications of Poly(Lactic Acid)/Poly(Lactic-Co-Glycolic Acid) Micro and Nanoparticles. *J. Pharm. Investig.* **2019**, *49* (4), 347–380. https://doi.org/10.1007/s40005-019-00439-x.

(51) Anderson, J. M.; Shive, M. S. Biodegradation and Biocompatibility of PLA and PLGA Microspheres. *Adv. Drug Deliv. Rev.* **2012**, *64* (SUPPL.), 72–82. https://doi.org/10.1016/j.addr.2012.09.004.

(52) Ghazali, N. M.; Samsudin, A. S. Progress on Biopolymer as an Application in Electrolytes System: A Review Study. *Mater. Today Proc.* **2020**, *49*, 3668–3678. https://doi.org/10.1016/j.matpr.2021.09.473.

(53) Zhang, W.; Li, H.; Yu, W. W.; Elezzabi, A. Y. Emerging Zn Anode-Based Electrochromic Devices. *Small Sci.* **2021**, *1* (12), 2100040. https://doi.org/10.1002/smsc.202100040.

(54) Cho, K. G.; Lee, J. I.; Lee, S.; Hong, K.; Kang, M. S.; Lee, K. H. Light-Emitting Devices Based on Electrochemiluminescence Gels. *Adv. Funct. Mater.* **2020**, *30* (33), 1907936. https://doi.org/10.1002/adfm.201907936.

(55) Sun, Q.; Li, Y.; Pei, Q. Polymer Light-Emitting Electrochemical Cells for High-Efficiency Low-Voltage Electroluminescent Devices. *J. Disp. Technol.* **2007**, *3* (2), 211–224. https://doi.org/10.1109/JDT.2007.896737.

(56) Tsuneyasu, S.; Jin, L.; Nakamura, K.; Kobayashi, N. An Electrochemically-Driven Dual-Mode Display Device with Both Reflective and Emissive Modes Using Poly(p-Phenylenevinylene) Derivatives. *Jpn. J. Appl. Phys.* **2016**, *55* (4). https://doi.org/10.7567/JJAP.55.041601.

(57) Kruszyna, H.; Kruszyna, R.; Hurst, J.; Smith, R. P. Toxicology and Pharmacology of Some Ruthenium Compounds: Vascular Smooth Muscle Relaxation by Nitrosyl Derivatives of Ruthenium and Iridium. *J. Toxicol. Environ. Health* **1980**, *6* (4), 757–773. https://doi.org/10.1080/15287398009529895.

(58) Kong, D.; Zhang, K.; Tian, J.; Yin, L.; Sheng, X. Biocompatible and Biodegradable Light-Emitting Materials and Devices. *Adv. Mater. Technol.* **2022**, *7* (2), 2100006. https://doi.org/10.1002/admt.202100006.

(59) Bizzarri, C.; Spuling, E.; Knoll, D. M.; Volz, D.; Bräse, S. Sustainable Metal Complexes for Organic Light-Emitting Diodes (OLEDs). *Coord. Chem. Rev.* **2018**, *373*, 49–82. https://doi.org/10.1016/j.ccr.2017.09.011.